RSC Advances

PAPER

View Article Online
View Journal | View Issue

Cite this: *RSC Adv.*, 2019, **9**, 5825

Phase transitions and chemical reactions of octahydro-1,3,5,7-tetranitro-1,3,5,7-tetrazocine under high pressure and high temperature†

Dexiang Gao,[a] Jin Huang,[a] Xiaohuan Lin,[a] Dongliang Yang,[b] Yajie Wang*[a] and Haiyan Zheng *[a]

Octahydro-1,3,5,7-tetranitro-1,3,5,7-tetrazocine (HMX) is one of the most important energetic materials. Investigations on its phase transitions and chemical reactions under extreme conditions are very important to understand the explosion process and design new energetic materials. By using a diamond anvil cell combined with *in situ* Raman, IR and X-ray diffraction techniques up to a pressure of ~40 GPa, we found that β-HMX undergoes four reversible phase transitions without any chemical reaction under external pressure at room temperature. Isostructural phase transitions emerge around 5 GPa (ζ-HMX) and 10–13 GPa (ε-HMX), and another two phases emerge at 16 GPa (η-HMX) and 27 GPa (ϕ-HMX). The unit cells of ζ-HMX and ε-HMX were determined as $a = 6.215$ Å, $b = 10.417$ Å, $c = 8.272$ Å, $\beta = 124.88°$, $P2_1/c$ at 6.2 GPa and $a = 6.130$ Å, $b = 9.846$ Å, $c = 8.258$ Å, $\beta = 125.06°$, $P2_1/c$ at 12.6 GPa, respectively. The crystal structures of β, ζ, and ε-HMX were obtained by Rietveld refinement, based on which the rotations of NO_2 groups were found to be related to the phase transition at 5 GPa. Additionally, HMX decomposes at 8.7 GPa and 300 °C. Carbon dioxide, hydroxyl, imino and hydroxyimino groups were detected in the IR spectrum, which indicates that the reaction contains a hydrogen transfer process. Our investigation uncovers the structural variation of β-HMX under external pressure and identifies the decomposition products under extreme conditions, which provides new insight to understand the detonation process of energetic materials.

Received 29th December 2018
Accepted 11th February 2019

DOI: 10.1039/c8ra10638j

rsc.li/rsc-advances

Introduction

Energetic materials are a class of materials which can release the stored chemical energy in a short time upon external stimulation, including heat, shock or electrical current. The process will generate pressure up to 50 GPa and temperature as high as 5500 K,[1] which will induce the energetic materials to transform into different phases and affect the reaction process. Thus, investigations on the phase evolution and the followed decomposition reaction of energetic materials under extreme conditions are critical to understand the real detonation process and will be beneficial for designing the new energetic materials with high energy density and improved safety.

Octahydro-1,3,5,7-tetranitro-1,3,5,7-tetrazocine (HMX) (Fig. 1a) is one of the widely used energetic materials. At ambient pressure, it has four polymorphs (α, β, γ and δ), which can be obtained by controlling the crystallization rate in solution.[2] The α, β and δ phases are pure crystalline phases, while the γ-HMX is a hydrate.[3] In practice, the sensitivity and the detonation velocity are very important parameters, which are closely related to the solid-state structure. Among the fourth phases, β-HMX is the most favourable phase for military energetic materials because of the highest density and the lowest

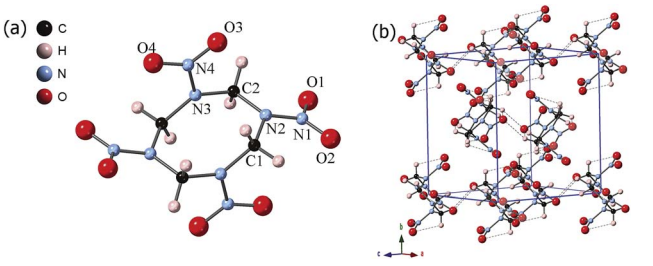

Fig. 1 The (a) molecular structure and (b) crystal structure of β-HMX at ambient condition. The dotted lines in (b) represent the inter/intra-molecular hydrogen bonds.

[a]*Center for High Pressure Science and Technology Advanced Research, 100094, Beijing, China. E-mail: yajie.wang@hpstar.ac.cn; zhenghy@hpstar.ac.cn*

[b]*Institute of High Energy Physics, Chinese Academy of Sciences, Beijing 100049, China*

† Electronic supplementary information (ESI) available: Table S1: assignments of Raman modes of β-HMX at ambient pressure, room temperature. Table S2: assignments of IR modes of β-HMX at 1.0 GPa, room temperature. Table S3: the refined cell parameters under non-hydrostatic pressure conditions. Table S4: atomic coordinates of HMX at 6.2 GPa. Table S5: atomic coordinates of HMX at 12.6 GPa. Fig. S1: pressure dependences of IR-active modes of β-HMX at ambient temperature. Fig. S2: torsion angles of axial NO_2 and equatorial NO_2 under non-hydrostatic pressure condition. See DOI: 10.1039/c8ra10638j

sensitivity.[1] At ambient condition, β-HMX (monoclinic, $P2_1/c$) is the most stable phase, with a unit cell $a = 6.54$ Å, $b = 11.05$ Å, $c = 8.70$ Å; $\beta = 124.3°$.[4] Its crystal structure including hydrogen atom positions was determined by neutron diffraction in 1970.[5] The β-HMX molecules are in chair conformation, with an inversion center at the center of the C_4N_4 ring. All of the four carbon atoms and two –N–NO_2 groups are approximately on the chair plane, and two opposite –N–NO_2 groups tilted above and below the plane, respectively. The molecules form rows of chairs with the interstitial site against the molecules of four neighbored rows (Fig. 1b). Each molecule has six intramolecular hydrogen bonds between the –NO_2 and –CH_2– groups, and 2–3 intermolecular hydrogen bonds for each –NO_2 group, which forms a network through the crystal. At 102–104 °C, β-HMX transforms to the α phase (orthorhombic, *Fdd*2)[4] and then to the δ phase (hexagonal, $P6_1$) when heated at 160–164 °C.[6] The HMX molecules in both α and δ phase adopt the boat conformation, which have all four nitro groups on one side of the molecular plane.

Goetz *et al.* reported that the β-HMX was stable up to 5.4 GPa at ambient temperature according to the *in situ* Raman and IR spectra.[7] By using the Raman spectroscopy and X-ray diffraction, Yoo *et al.* investigated the phase evolution of the β-HMX under both quasi-hydrostatic condition to 45 GPa and non-hydrostatic condition to 10 GPa.[8] The pressure-volume relation displays two phase transitions under quasi-hydrostatic compression: one is at 12 GPa with no apparent volume change (ε-HMX) and the other is at 27 GPa with a 4% volume change (ϕ-HMX). Under non-hydrostatic condition, the chemical reaction was reported at 6 GPa as the strong increase of the background. Besides these two, Michael Pravica *et al.* reported another transition occurring near 5 GPa under non-hydrostatic condition.[9] They also proposed that at 25 GPa HMX probably transformed to the known δ phase and there is no chemical reaction detected up to 30 GPa at room temperature. By using the isentropic compression experiment technique, D. E. Hare *et al.* pointed out no obvious indication of the phase transition processing at 27 GPa.[10] By using the same technique to compress HMX single crystals up to 50 GPa, Hooks. *et al.* also didn't find any evidences for the phase transition in 27 GPa.[11] Theoretically, by using isothermal–isobaric molecular dynamics (NPT-MD) simulation, an abrupt change for the volume and internal geometrical parameters was observed at 27 GPa suggesting a phase transition.[12] Lei Zhang *et al.* employed the first-principles method to predict that no β–δ/ε–δ phase transition occurs at 27 GPa.[13] When heated at high pressure, the β-HMX decomposes or after a phase transition to δ-HMX experimentally.[14] Debashits Chakraborty *et al.* proposed three reaction mechanisms in the gas phase HMX according to the *ab initio* calculations, including the homolytic cleavage of N–N bond to form NO_2, the eliminations of HONO and the O-migration from one of the NO_2 groups to neighbouring C atom.[15] Gasper J. Piermarini *et al.* reported that the pressure decreases the rate of thermal decomposition and they concluded that there might involve a ring expansion prior to bond scission.[16] By employing the *in situ* infrared (IR) spectroscopy, N_2O and CO_2 were identified in the decomposition products and they found the pressure accelerates the decomposition at low-to-moderate pressure and decelerates the reaction at higher pressure.[14]

Although HMX has been studied and used for at least 60 years, the phase transitions of β-HMX under extreme conditions were still controversial and its reaction mechanism is still not clear. All the known researches on the phase relation are based on the *P*–*V* relations or the spectral results, lack of crystallographic results even in the low pressure range, which is actually very important to understand the structure evolution and chemical reaction. Furthermore, for the decomposition process, there are still no enough information about the products of HMX under variable high pressure and high temperature conditions.

In this paper, by combing multiple technologies including *in situ* Raman, IR, and X-ray diffraction (XRD), we investigated the phase transitions and decomposition of β-HMX under non-hydrostatic pressure up to 40 GPa. Four new phases named ζ-HMX, ε-HMX, η-HMX and ϕ-HMX were indentified and the crystal structures of β, ζ and ε-HMX were determined. We found the rotation of NO_2 groups was closely related to the phase transition at 5 GPa from β to ζ-HMX. Additionally, HMX is decomposed at 8.7 GPa and 300 °C, and produces carbon dioxide, hydroxyl, imino and hydroxyimino groups, which indicates that the reaction contains the hydrogen transfer process.

Experimental methods

The HMX sample used for the Raman, IR and synchrotron XRD measurements was gently ground in an agate mortar. The sample was identified as β-HMX by powder XRD analysis on a PANalytical Empyrean diffractometer (Cu Kα radiation), and no impurity was detected. A symmetric diamond anvil cell with $d_{culet} = 300$ μm was employed to apply pressure. For the *in situ* IR measurement, a pair of type II diamonds was used. A T-301 stainless steel gasket was pre-indented to a thickness of 40 μm and a hole with diameter of 100 μm was drilled to serve as the sample chamber. *In situ* Raman spectra were collected on a commercial Renishaw Raman microscope with excitation laser wavelength at 488 nm. *In situ* IR experiments were carried out on a Bruker VERTEX 70v with HYPERION 2000 microscope. A Globar was used as a conventional source. The spectra were collected in a transmission mode in the range of 600–4000 cm^{-1} with a resolution of 2 cm^{-1}. The aperture was set to 20×20 μm^2 and the absorption of the diamond anvils of the same area was used as the background. No pressure media was added during the Raman and IR measurements. For the *in situ* IR measurements under high pressure and room temperature, KBr pellet was used to optimize the thickness of the sample for good absorption signals. The *in situ* IR spectra of HMX without KBr were also measured and no difference was observed.

A resistive heater was wrapped around the cell for heating and the temperature was measured by using a calibrated thermocouple (K-type) placed on the gasket. To avoid the interference of KBr, pure HMX was loaded into the gasket when measuring the IR spectra under high pressure and high temperature conditions. The sample was compressed to

~6.6 GPa and heated up to 200 °C and 300 °C, respectively. The IR spectra were collected after cooling down to the room temperature.

In situ high pressure angular-dispersive X-ray diffraction (ADXRD) data up to 40 GPa were collected at the High Pressure Station at 4W2 beamline of the Beijing Synchrotron Radiation Facility (BSRF). The incident X-ray was monochromated to 0.6199 Å and a Pilatus detector calibrated by a CeO_2 standard sample was used. The beam size was ~20 × 30 μm^2. The data was reduced by using the Dioptas software.[17] The pressures of the *in situ* Raman, IR spectroscopy and XRD measurements were calibrated by the ruby fluorescence.[18] The crystal structures and atomic positions of β-HMX under high pressure were determined by Rietveld refinement using the Jana 2006 package.[19]

Results and discussion

Raman spectra of β-HMX under non-hydrostatic high pressure

Fig. 2 displays Raman spectra of β-HMX under non-hydrostatic pressure condition up to 40 GPa. The frequency shifts of the Raman modes with increasing pressure are shown in Fig. 3. The Raman modes at ambient pressure are assigned according to the calculated results of the reference and shown in Table S1.†[20] The peaks below 400 cm^{-1} correspond to the interspersed lattice phonons. The peaks related to the C_4N_4 ring are mainly in the following regions: (1) distortions and deformations of the C_4N_4 ring (400–800 cm^{-1}); (2) C–N stretching of the C_4N_4 ring (ring-stretching motion) and N–N stretching (800–1240 cm^{-1});

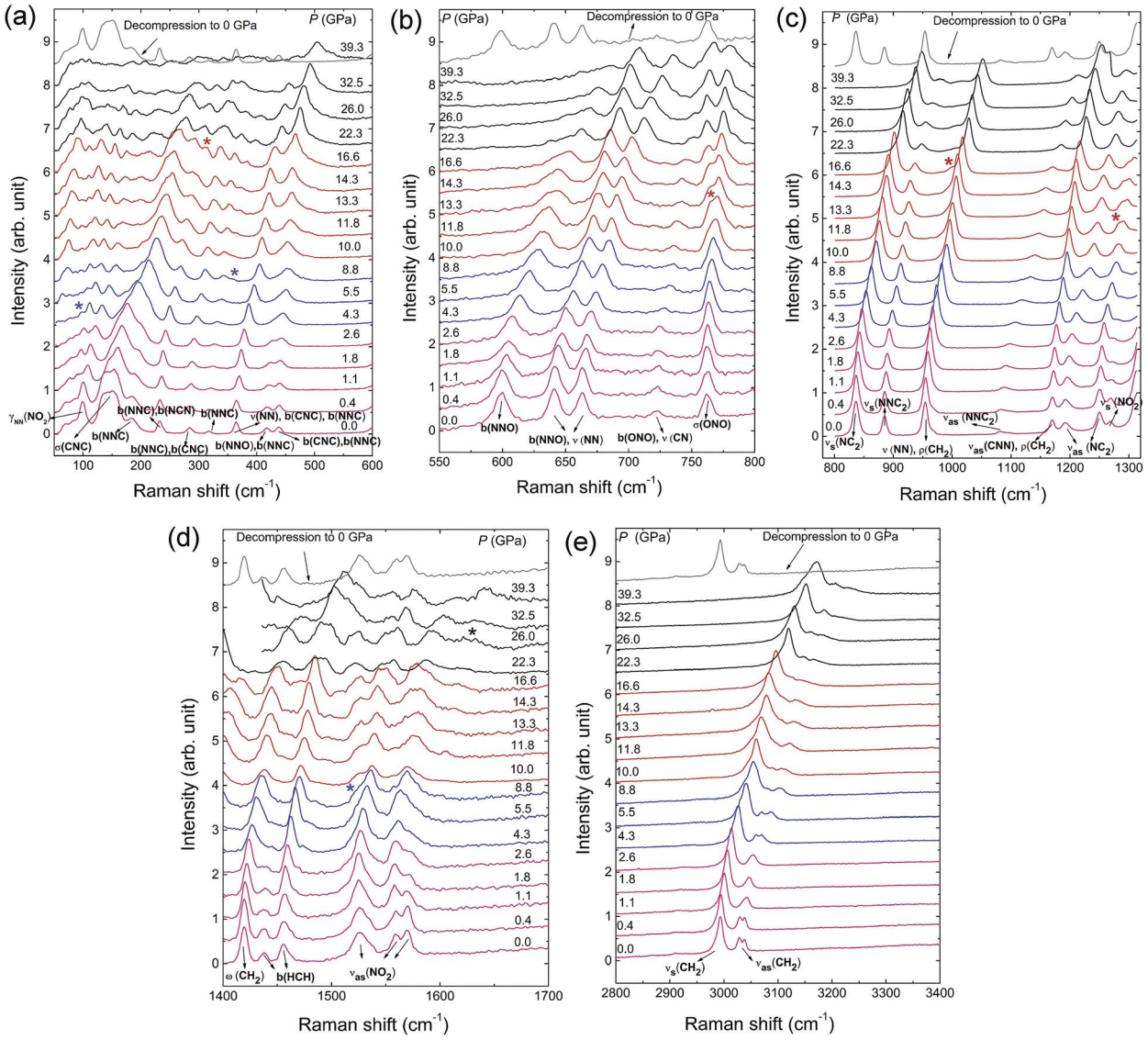

Fig. 2 Raman spectra of β-HMX under non-hydrostatic pressure up to 40 GPa and ambient pressure after decompression. (a) 100–600 cm^{-1}, (b) 550–800 cm^{-1}, (c) 800–1300 cm^{-1}, (d) 1400–1700 cm^{-1}, (e) 2800–3400 cm^{-1} at selected pressures. The new peaks are marked by the asterisks. The Raman modes abbreviations are as following: *b*(XYZ): X–Y–Z bending vibration; ν_{as}(XY$_2$): Y–X–Y asymmetric stretching vibration; ν_{as}(XXY$_2$): X–X–Y$_2$ asymmetric stretching vibration; ν_s(XY$_2$): Y–X–Y symmetric stretching vibration; ν_s(XXY$_2$): X–X–Y$_2$ symmetric stretching vibration; ρ(XY$_2$): XY$_2$ rocking vibration in XY$_2$ plane; σ(XY$_2$): X atom rocking vibration out of XY$_2$ plane; ω(XY$_2$): Y$_2$ rocking vibration out of XY$_2$ plane; γ_{NN}(XY$_2$): XY$_2$ twisting vibration about N–N bond.[20]

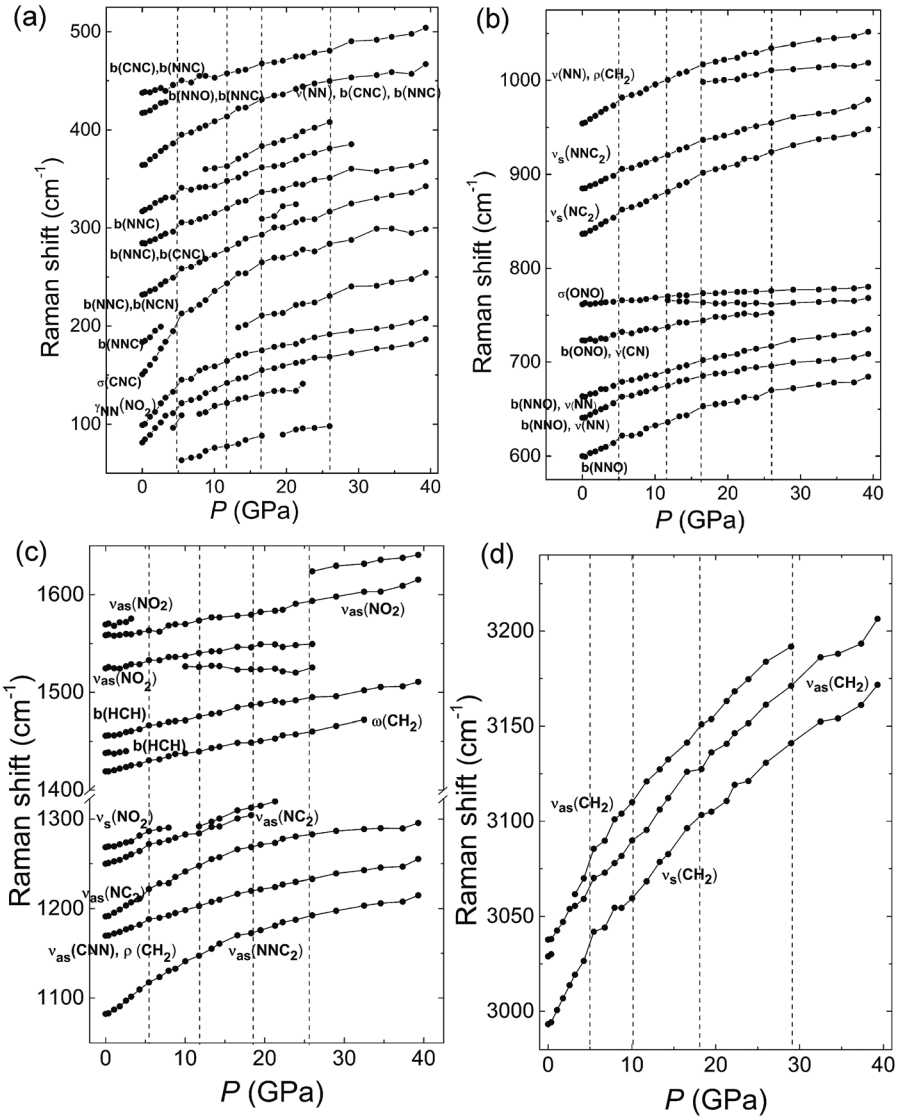

Fig. 3 Raman frequency shifts of β-HMX at room temperature as a function of pressure in the range of (a) 100–500 cm^{-1}, (b) 600–1050 cm^{-1}, (c) 1050–1650 cm^{-1}, and (d) 3000–3250 cm^{-1}. The symbol of the different vibration modes can be found in the caption of Fig. 2. Four vertical lines represent boundaries of different phases. Raman spectra of β-HMX under non-hydrostatic high pressure.

(3) deformation of CH_2 moieties in C_4N_4 ring (1350–1500 cm^{-1}); (4) C–H bond stretching (2900–3100 cm^{-1}). For the NO_2 moieties, two kinds of modes are observed in the Raman spectra, one is the distortion mode at 762 cm^{-1} and the others are the stretching modes, the symmetric (1269 cm^{-1}) and asymmetric stretches (1526–1570 cm^{-1}). Upon compression, all the Raman modes show obvious blue shifts because of the increasing interatomic interactions.[21] As shown in Fig. 2, at low pressure region below 5 GPa, a new peak marked by asterisks appears at 98 cm^{-1} around 4.3 GPa. Meanwhile, as displayed in Fig. 3, a discontinuity is observed at 5 GPa. It indicates the phase transition from β-HMX to ζ-HMX. Additionally, it also should be noticed that the two peaks assigned to H–C–H asymmetric stretching (3028 cm^{-1} and 3036 cm^{-1}) shift to high frequency at different rates (Fig. 3d). The low frequency H–C–H asymmetric stretching mode shifts faster than the high frequency one, which makes these two peaks overlap at 1.1 GPa and then separate at 3.2 GPa. This suggests that the H–C–H asymmetric stretching mode at low frequency is more sensitive to pressure. By further compression, several distinct changes are observed above 8.8 GPa, including a new mode (360 cm^{-1}) next to the bending mode of the N–N–C or N–N–O bond and a new peak at 1525 cm^{-1} on the shoulder of $\nu_{as}(NO_2)$ (asymmetric stretches of the NO_2 moieties). The new peak at 1525 cm^{-1} shows red shift upon further compression, which is probably attributed to the strengthened intermolecular hydrogen bond during compression.[22] Furthermore, the peaks (765 cm^{-1} and 1285 cm^{-1}) ascribed to the σ(ONO) (O–N–O wagging vibration) and $\nu_{as}(NC_2)$ (the asymmetric stretches of the C–N–C bond) split significantly when compressed to 11.8 GPa. The shoulder in the low frequency of σ(ONO) also shows red shift upon further compression. All the new modes indicate that the second phase transition from ζ-HMX to ε-HMX occurs. The phase transition is very sluggish over a broad pressure range from 8.8 to 11.8 GPa.

This may be because of the non-hydrostatic pressure condition, or the limited difference between their Gibbs free energies. With further compression, the third phase transition from ε-HMX to η-HMX emerges at 16.6 GPa. Above 16.6 GPa, a new peak emerges at 312 cm^{-1} at the low frequency side of N–N–C (or C–N–C) bending modes. Meanwhile, a shoulder in the region of the N–N stretching modes emerges at 1000 cm^{-1}. At 26 GPa, a very weak new peak can be found around 1600 cm^{-1} and a lot of peaks disappeared at this pressure (Fig. 3), this might suggest another phase transition from η-HMX to ϕ-HMX. Solid evidences of this phase transition can be found from the *in situ* XRD data shown below and consistent with the literatures.[8,9]

Therefore, from the *in situ* Raman spectra under high pressure, four phase transitions are concluded with the transition boundaries at 4.3 GPa, 12 GPa, 17 GPa and 26 GPa. When decompressed to ambient pressure, the Raman spectrum is the same as that collected before compression. This suggests that all the phase transitions are reversible and there is no chemical reaction happened up to 39.3 GPa under non-hydrostatic pressure condition. All the phase transitions are related to the bending or stretching modes of the N–N–C, C–N–C or NO_2. This suggests that these phase transitions rise from the distortion of the C_4N_4 ring of the HMX, which may result in the reorientation of the NO_2 groups. More evidences are discussed later in the *in situ* high pressure IR and XRD investigations. The red shift of the new peaks related to stretching mode ($\nu_{as}(NO_2)$) and wagging vibration (σ(ONO)) of NO_2 moieties indicates the enhancement of hydrogen bonds of NO_2 during compression.

IR spectra of β-HMX under non-hydrostatic high pressure

In situ IR spectra were also collected under non-hydrostatic pressure condition up to 40.2 GPa. Table S2† gives the assignment of the IR modes of the β-HMX at 1.0 GPa according to the calculation results of the ref. 20 In the region from 604–660 cm^{-1}, the peaks are mainly from distortions and deformations of the C_4N_4 ring, including the bending of N–N–O angles and the stretching of N–N bonds. The peaks located in the region of 700–800 cm^{-1} are ascribed to the distortion of the ring and NO_2 moieties. Except for the peak at 937 cm^{-1}, all the peaks in the region 800–970 cm^{-1} are related to the C–N stretching of the C_4N_4 ring (ring stretching motion) and the peaks in the region of 970–1240 cm^{-1} are recognized as the stretching of N–N and C–N bonds. The peaks in 1350–1500 cm^{-1} are related to the deformation of CH_2 in C_4N_4 ring. The peaks in 1500–1700 cm^{-1} and 2900–3100 cm^{-1} are ascribed to the asymmetric stretches of the $-NO_2$, and the C–H bond stretching respectively.

As displayed in Fig. 4, no remarkable changes are observed in the IR spectral patterns but shift to high frequency below 12 GPa. Above 12.2 GPa, a shoulder peak (978 cm^{-1}) in the region of ν_{as}(NNC) (the asymmetric stretches of the N–N–C) is observed. Meanwhile, a new mode emerges at 665 cm^{-1} in high-frequency region of N–N–O bending vibration and two peaks appear in the shoulder of $\nu_s(NO_2)$ at 1338 cm^{-1} and 1612 cm^{-1}. The results correspond to the phase transition from ζ-HMX to ε-HMX. All the changes are related to the NO_2 moieties, suggesting the phase transition may contain the distortion of the NO_2 groups. Under further compression to 17.1 GPa, a new peak (1479 cm^{-1}) next to the bending mode of the H–C–H emerges, while several peaks (773 cm^{-1}, 876 cm^{-1}) disappear around 17.1 GPa. This corresponds to the transition from ε-HMX to η-HMX. After decompression from 40 GPa, all of the peaks are the same as the β-HMX, which also indicates all the phase transitions in our experiment are reversible without any chemical reactions. The frequency shifts of the IR modes with increasing pressures are shown in Fig. S1.† Similar to the Raman results, as Fig. S1c† displayed, the two peaks assigned to H–C–H

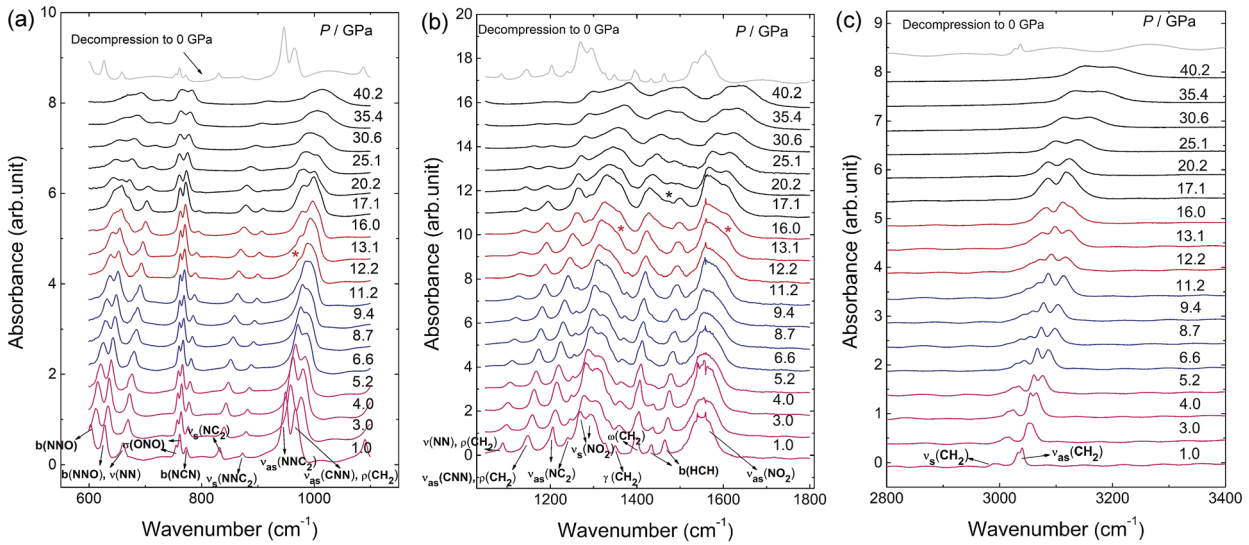

Fig. 4 *In situ* IR spectra of β-HMX under non-hydrostatic pressure condition up to 40 GPa and ambient pressure after decompression in the spectra region of (a) 600–1100, (b) 1050–1800 and (c) 2800–3400 cm^{-1} at selected pressures. The new peaks are marked by the asterisks. The IR modes abbreviations are the same as the Raman modes shown in Fig. 2. $\gamma(XY_2)$: XY_2 twisting vibration about bisector of Y–X–Y angle.

asymmetric stretching display different frequency trends dependent on the pressures. The peak of low frequency moves to high wave number at a higher rate than the one of high frequency. Besides, during compression, two discontinuities are observed at ~5 GPa and 13 GPa confirming the phase transition from β-HMX to ζ-HMX and ζ-HMX to ε-HMX respectively. Additionally, according to Fig. S1b and c,† the discontinuities emerge at ~27 GPa. Several modes, $\nu_{as}(NNC_2)$, $b(NNO)$, $\nu_{as}(NC_2)$, $\nu(NN)$, $\rho(CH_2)$, $\nu_{as}(CNN)$, $\nu_{as}(NO_2)$, and $\nu_s(CH_2)$ shift to low frequency obviously around 27 GPa and then shift to high frequency again, which indicates another phase transition from η-HMX to ϕ-HMX. The result agrees well with Raman spectra and XRD data indicated below.

X-ray diffraction of β-HMX under non-hydrostatic pressure

To investigate the structural variation of the phases under high pressure, XRD patterns of β-HMX under non-hydrostatic pressure were collected up to 40.7 GPa (Fig. 5). All the peaks slowly shift to high-angle below 10.6 GPa upon compression. Above 10.6 GPa, the −102 peak gradually shifts to low-angle, which corresponds to the phase transition to ε-HMX. At 16.9 GPa, a new peak marked by the asterisk emerges at low-angle, which evidences the phase transition to η-HMX. With further compression above 26.2 GPa, the −102 peak shifts to high-angle. The −132 peak shifts to high-angle from 16.9 to 26.2 GPa at a very fast rate, and slows down above 26.2 GPa. These features are related to the phase transition to ϕ-HMX. All of the diffractions are significantly weakened above 16.9 GPa, but still observable up to 40.7 GPa, indicating that the phase ϕ-HMX remains stable up to 40.7 GPa. The XRD pattern of sample decompression from 40.7 GPa is just the same as the starting material, which indicates these transitions are reversible. No chemical reaction can concluded from the compression–decompression cycle.

Rietveld refinement was performed to determine the crystal structures. The original structural model of β-HMX are from a previous investigation ($P2_1/n$, $a = 6.54$ Å, $b = 11.05$ Å, $c = 7.37$ Å; $\beta = 102.8°$).[23] The lattice parameters from 0.2 GPa to 14.5 GPa are shown in Table S3† and Fig. 6a. The b-axis has the highest compressibility. This is because several hydrogen bonds lie in or close to the ac-plane. The pressure depending unit cell volume was plotted and fitted using the 3rd order Brich–Murnaghan equation of state:[24,25]

$$P(V) = 1.5B_0\left[\left(\frac{V_0}{V}\right)\frac{7}{3} - \left(\frac{V_0}{V}\right)\frac{5}{3}\right]\left\{1 + \frac{3}{4}(B1 - 4)\left[\left(\frac{V_0}{V}\right)\frac{2}{3} - 1\right]\right\}$$

B_0 and B_1 are ambient bulk modulus and its derivative, V_0 is the unit cell volume at ambient conditions, and all of them are released for fitting. As displayed in Fig. 6b, the volumes at 5.1 GPa and 10.6 GPa are discontinuous compared with other points, so we use two curves to fit the data, respectively. From 0.2 GPa to 4.2 GPa, $V_0 = 521.6 \pm 3.5$ Å^3, $B_0 = 14.4 \pm 4.2$ GPa, $B_1 = 12.8 \pm 5.5$. From 6.2 to 9.1 GPa, $V_0 = 482.7 \pm 1.4$ Å^3, $B_0 = 65.1 \pm$

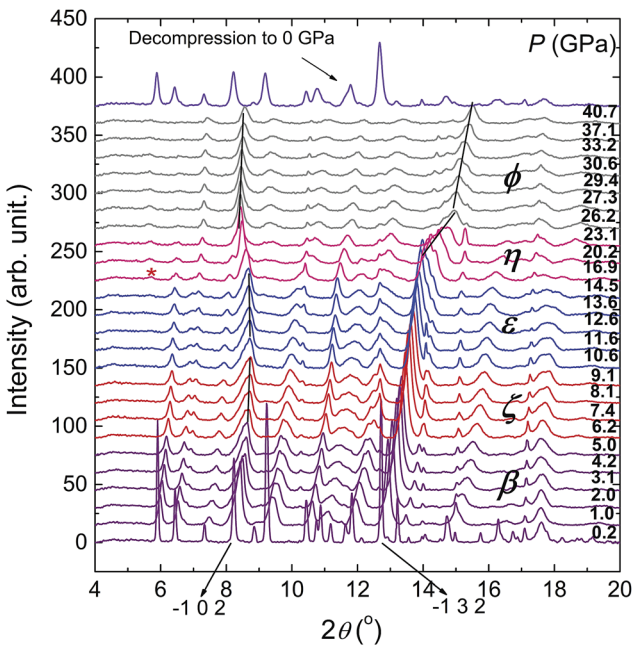

Fig. 5 XRD patterns of β-HMX under non-hydrostatic pressure up to 40.7 GPa and ambient pressure after decompression. The corresponding phases are noted in the figure.

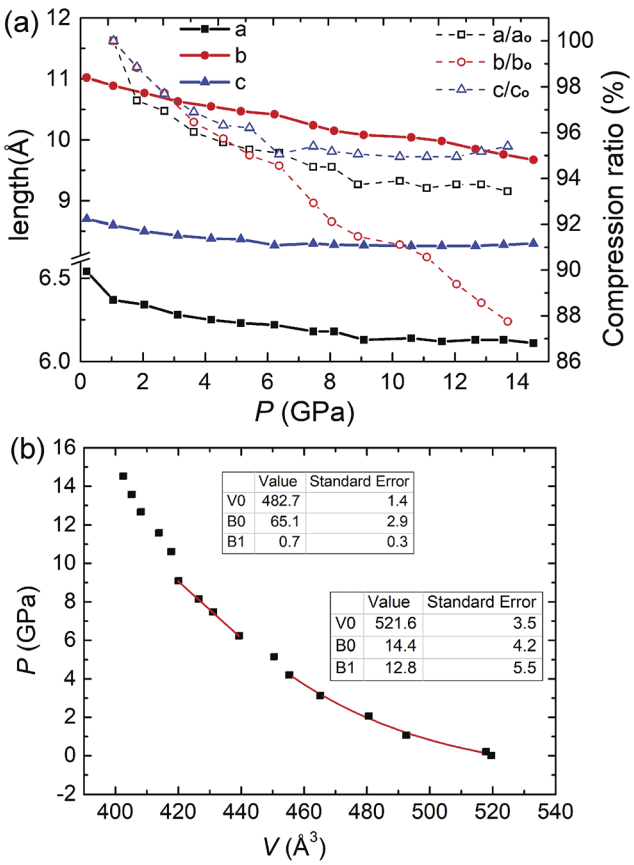

Fig. 6 (a) Variations in cell parameters as a function of pressures and compression ratios of three axes. (b) Equation of state of β-HMX under non-hydrostatic pressure. Two different lines are displayed in the figure. The error bar is smaller than the square.

2.9 GPa, $B_1 + 0.7 \pm 0.3$. The significant difference between the V_0 and B_0 values clearly indicates a phase transition from β-HMX to ζ-HMX at around 5 GPa, which is in consistence with the spectral experiment. The unit cell of ζ-HMX at 5.1 GPa is a = 6.233 Å, b = 10.474 Å, c = 8.369 Å, β = 124.49°, $P2_1/c$. For the ε-HMX, the lattice parameters are a = 6.130 Å, b = 9.846 Å, c = 8.258 Å, β = 125.06°, $P2_1/c$ at 12.6 GPa. The atomic positions of ζ-HMX and ε-HMX are displayed in Tables S4 and S5.† Above 10.6 GPa, the uncertainties of the refined parameters are too big to get reliable equation of state.

There are 10 crystallographic independent atoms (exclude hydrogen) in β-HMX, and hence 30 independent atomic coordinates (x, y and z for each atom), which are too many to be fitted. To reduce the degree of freedoms, we introduced semi-rigid body in the refinement. The N–N, N–O and C–N bond length are restrained to 1.36 Å, 1.225 Å and 1.45 Å. The bond angles of O–N–O and O–N–N are restrained to 120°. The bond angles of C–N–C, N–C–N and N–N–C are restrained to 122°, 111° and 119°, respectively according to the literature.[5] Hydrogen atoms were automatically added by the program and fixed on the carbon atoms. In the semi-rigid body, the C_4N_4 ring is still free for distortion and the NO_2 groups can also rotate, but the molecule won't be broken. Fig. 7a displays the molecular structures of ambient pressure and 6.2 GPa, respectively. Compared with that at ambient pressure, the molecular structure at 6.2 GPa abruptly distorts. By measuring the angle between two skew lines (C1′–C2 and O3–O4), we found the axial NO_2 group rotates approximately 23.3° around the N–N bond compared with that at previous pressure point (5.1 GPa, Fig. S2†). The rotation of NO_2 group may be the direct reason or result of the β–ζ phase transition around 5 GPa.

The intermolecular and intramolecular hydrogen bonds (Fig. 7b) are closely associated with the moving of nitro groups.

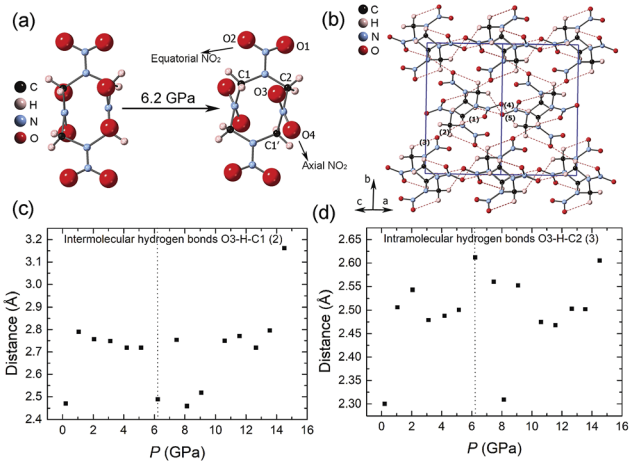

Fig. 7 Molecular structures of (a) ambient pressure (left) and 6.2 GPa (right). (b) Hydrogen bonds inside β-HMX crystal at ambient pressure. Red dotted lines represent hydrogen bonds. (1) and (3) are intramolecular hydrogen bonds. (2), (4) and (5) are intermolecular hydrogen bonds. Most hydrogen bonds approximately lie on the ac plane. (c) and (d) The lengths of hydrogen bonds (O···H) (2) and (3) under high pressure.

The variations of five hydrogen bonds with pressure are shown in Fig. 7c, d and S3.† Compared with the intramolecular hydrogen bonds, the intermolecular hydrogen bonds are more compressible. Below 5.1 GPa, the lengths of hydrogen bonds change smoothly. At 6.2 GPa, the length of intermolecular hydrogen bonds related to O3 (hydrogen bond 2, Fig. 7c) decreases and the length of intramolecular hydrogen bonds related to O3 (hydrogen bond 3, Fig. 7d) increases abruptly, which indicates the axial nitro rotates at this pressure condition. Above 6.2 GPa, the lengths of hydrogen bonds are more diverging, which is likely to be related to the β–ζ phase transition and the changing of molecular conformation around 5 GPa.

Decomposition of HMX under non-hydrostatic pressure condition and high temperature

Because no chemical reaction of HMX is observed at high pressure (up to 40 GPa) and room temperature, we use diamond anvil cell (DAC) combing with resistive heating system to explore its chemical reaction under extreme conditions. Fig. 8 display the IR spectra of HMX under high pressure conditions after heating at 200 °C and 300 °C. At 6.6 GPa, after heating at 200 °C, the pattern has no remarkable difference compared with the one before heating, suggesting no chemical reaction happened (Fig. 8a). By heating the sample at 300 °C, as shown in the inset photos of Fig. 8a, the colour of HMX changes from white to black and the pressure changes from 6.6 GPa to 8.7 GPa. All the signals of HMX disappeared and four new peaks were observed. The two peaks centered at 2396 cm^{-1} and 3767 cm^{-1} arise from the asymmetric stretch (ν_3) and the combination mode ($\nu_1 + \nu_3$) of solid CO_2, respectively.[26] The peaks appeared at 3500 cm^{-1} and 3200 cm^{-1} are tentatively assigned to the stretching of –OH and –NH or –NOH groups.[27] The appearance of hydroxyl, imino and hydroxyimino groups indicates that the hydrogen transfer process is included in the decomposition process under high temperature and high pressure conditions. This is consistent with the *ab inito* study of HMX, which shows formation of the HONO group may be the initiation mechanism of the decomposition reaction.[15] This hydrogen transfer process is also confirmed in the process of nitromentane decomposition under high static pressure and hydrogen transfer to form the aci-ion ($CH_2NO_2^-$) mechanism is thus proposed.[27]

Upon decompression, the IR spectra of the decomposition product changes substantially as shown in Fig. 8b. When decompressed to 5.5 GPa, the peaks centered at 814 cm^{-1}, 1095 cm^{-1}, 1314 cm^{-1}, 1469 cm^{-1} and 1628 cm^{-1} become more obvious and most of these peaks can still be observed when the DAC was open, which means these absorption bands come from the solid decomposition products. When the pressure decreases to 2.1 GPa, the peaks assigned to the –OH and –NH or –NOH groups develops to a broad peak centered at 3246 cm^{-1} and it disappears at 0.6 GPa or opening the cell. This means these peaks related to the –OH and –NH or –NOH groups may come from highly volatile small molecules. The Raman spectrum of the remained black solid exhibits two broad bands centered at

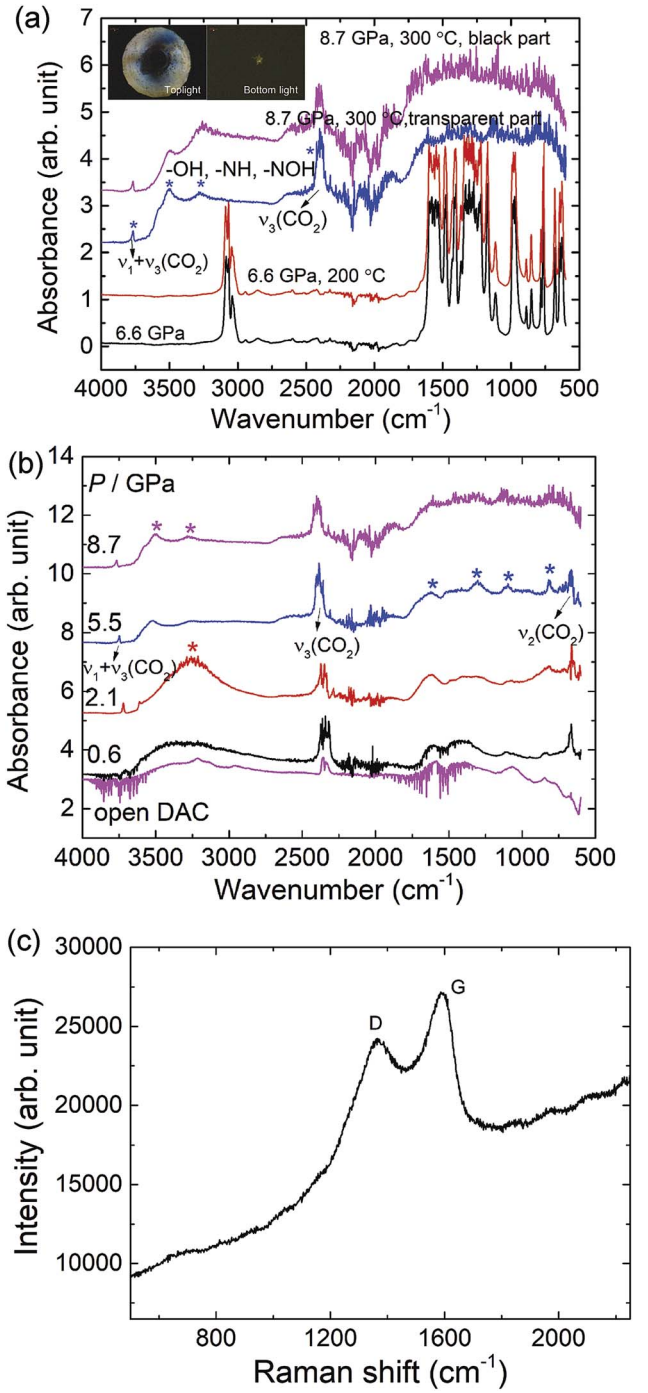

Fig. 8 (a) Infrared absorption spectra of HMX under high pressure, room temperature and after heating at 200 °C and 300 °C. All the spectra were measured at room temperature. The black and transparent area can be observed after heating at 300 °C and 8.7 GPa (inset pictures); (b) the IR spectra of the transparent area during decompression process; (c) the Raman spectrum of the black product remained on the diamond culet after opening the DAC.

1371 cm^{-1} and 1587 cm^{-1} at ambient conditions as shown in Fig. 8c, similar with the diamond (D) and graphite (G) of disordered graphite,[28] which means the black product is most likely a framework material similar to that of a "disordered" graphite.[28]

Conclusion

Combining with *in situ* Raman, IR spectroscopy, and X-ray diffraction, a systematic study of phase transitions and chemical reactions of β-HMX under high pressure and high temperature was conducted in this work. Four phases transitions at 5 GPa (ζ-HMX), 12 GPa (ε-HMX), 16 GPa (η-HMX) and 27 GPa (ϕ-HMX) were determined at high pressure and room temperature. The rotations of the NO_2 groups under high pressure are related to the first phase transition β–ζ occurring around 5 GPa. All of them are reversible without any chemical reactions below 40 GPa. At 8.7 GPa and 300 °C, HMX decomposes to the disordered graphite like black product, highly volatile small molecules with –OH, –NH or –NOH groups and carbon dioxide. The decomposition process contains hydrogen transfer process. Our studies clarify the controversy on the phase transition of β-HMX under high pressure, especially the phase transition at 27 GPa, which has been a long hot debate. The decomposition products under extreme conditions were also given out and described in details. This will give new insights to understand the actual detonation process of energetic materials, which will be beneficial for designing new explosive materials with tailored properties.

Conflicts of interest

There are no conflicts to declare.

Acknowledgements

This work is supported by Science Challenge Project, no. TZ2016001. The authors also acknowledged the support of the National Nature Science Foundation of China (NSFC) (grant no. 21601007 and 21875006). The high pressure *in situ* X-ray diffraction was performed at 4W2 HP-Station, Beijing Synchrotron Radiation Facility (BSRF), which is supported by Chinese Academy of Sciences (Grant KJCX2-SW-N20, KJCX2-SW-N03). The authors also thank Dr Yanqing Wu for providing the β-HMX.

Notes and references

1 F. P. A. Fabbiani and C. R. Pulham, *Chem. Soc. Rev.*, 2006, **35**, 932–942.
2 W. C. Mccrone, *Anal. Chem.*, 1950, **22**, 1225–1226.
3 P. Main, R. E. Cobbledick and R. W. H. Small, *Acta Crystallogr.*, 1985, **C41**, 1351–1354.
4 H. H. Cady, A. C. Larson and D. T. Cromer, *Acta Crystallogr.*, 1963, **16**, 617–623.
5 S. C. Chang and P. B. Henry, *Acta Crystallogr.*, 1970, **B26**, 1235–1240.
6 R. E. Cobbledick and R. W. H. Small, *Acta Crystallogr.*, 1974, **B30**, 1918–1922.
7 F. Goetz, T. B. Brill and J. R. Ferraro, *J. Phys. Chem.*, 1978, **82**, 1912–1917.
8 C.-S. Yoo and H. Cynn, *J. Chem. Phys.*, 1999, **111**, 10229.

9 M. Pravica, M. Galley, E. Kim, P. Weck and Z. Liu, *Chem. Phys. Lett.*, 2010, **500**, 28–34.
10 D. E. Hare, J. W. Forbes, D. B. Reisman and J. J. Dick, *Appl. Phys. Lett.*, 2004, **85**, 949–951.
11 D. E. Hooks, D. B. Hayes, D. E. Hare, D. B. Reisman, K. S. Vandersall, J. W. Forbes and C. A. Hall, *J. Appl. Phys.*, 2006, **99**, 124901.
12 L.-Y. Lu, D.-Q. Wei, X.-R. Chen, G.-F. Ji, X.-J. Wang, J. Chang, Q.-M. Zhang and Z.-z. Gong, *Mol. Phys.*, 2009, **107**, 2373–2385.
13 L. Zhang, S.-L. Jiang, Y. Yu, Y. Long, H.-Y. Zhao, L.-J. Peng and J. Chen, *J. Phys. Chem. B*, 2016, **120**, 11510–11522.
14 E. A. Glascoe, J. M. Zaug and A. K. Burnham, *J. Phys. Chem. A*, 2009, **113**, 13548–13555.
15 D. Chakraborty, R. P. Muller, S. Dasgupta and W. A. Goddard, *J. Phys. Chem. A*, 2001, **105**, 1302–1314.
16 G. J. Piermarini, S. Block and P. J. Miller, *J. Phys. Chem.*, 1987, **91**, 3872–3878.
17 C. Prescher and V. B. Prakapenka, *High Pressure Res.*, 2015, **35**, 223–230.
18 H. K. Mao, J. Xu and P. M. Bell, *J. Geophys. Res.*, 1986, **91**, 4673–4676.
19 V. Petricek, M. Dusek and L. Palatinus, *Z. Kristallogr.*, 2014, **229**, 345–352.
20 H. V. Brand, R. L. Rabie, D. J. Funk, I. Diaz-Acosta, P. Pulay and T. K. Lippert, *J. Phys. Chem. B*, 2002, **106**, 10594–10604.
21 Y. Gu, K. Wang, Y.-X. Dai, G. Xiao, Y. Ma, Y. Qiao and B. Zou, *J. Phys. Chem. Lett.*, 2017, **8**, 4191–4196.
22 G. Qi, K. Wang, G. Xiao and B. Zou, *Sci. China Chem.*, 2018, **61**, 276–280.
23 P. F. Eiland and R. Pepinsky, *Z. Kristallogr.*, 1955, **106**, 273–298.
24 F. Birch, *Phys. Rev.*, 1947, **71**, 809–824.
25 F. Birch, *J. Geophys. Res.: Atmos.*, 1978, **83**, 1257–1268.
26 R. Lu and A. M. Hofmeister, *Phys. Rev. B: Condens. Matter Mater. Phys.*, 1995, **52**, 3985–3992.
27 M. Citroni, R. Bini, M. Pagliai, G. Cardini and V. Schettino, *J. Phys. Chem. B*, 2010, **114**, 9420–9428.
28 S. Reich and C. Thomsen, *Philos. Trans. R. Soc., A*, 2004, **362**, 2271–2288.